Robust Optimal Sun-Pointing Control of a Large Solar Power Satellite

Shunan Wu[a], Kaiming Zhang[a], Haijun Peng[b], Zhigang Wu[a], Gianmarco Radice[c]

[a]School of Aeronautics and Astronautics, Dalian University of Technology, 116024 Dalian, People's Republic of China
[b]Department of Engineering Mechanics, Dalian University of Technology, 116024 Dalian, People's Republic of China
[c]School of Engineering, University of Glasgow, Glasgow G12 8QQ, UK

[*]Corresponding author: Tel./fax: +86 411 84706772. E-mail address: wuzhg@dlut.edu.cn (Zhigang Wu)

ABSTRACT

The robust optimal sun-pointing control strategy for a large geostationary solar power satellite (SPS) is addressed in this paper. The SPS is considered as a huge rigid body, and the sun-pointing dynamics are firstly proposed in the state space representation. The perturbation effects caused by gravity gradient, solar radiation pressure and microwave reaction are investigated. To perform sun-pointing maneuvers, a periodically time-varying robust optimal LQR controller is designed to assess the pointing accuracy and the control inputs. It should be noted that, to reduce the pointing errors, the disturbance rejection technique is combined into the proposed LQR controller. A recursive algorithm is then proposed to solve the optimal LQR control gain. Simulation results are finally provided to illustrate the performance of the proposed closed-loop system.

Keywords: Solar power satellite; Space solar power station; Attitude dynamics; Optimal control; LQR

1. Introduction

Recent years have witnessed the resurgence of space-based solar power research, and in particular the solar power satellite (SPS) paradigm has received much attention due to its potential for generating large amounts of clean electrical power. The SPS concept, firstly proposed by Peter Glaser in 1968 [1], consists of three main components: a solar array to collect solar radiation and convert it into direct current (DC) electricity, a DC-to-microwave converter and an antenna that directs a microwave beam towards the surface of the Earth. The main benefits of a SPS as opposed to a solar power system on the ground are that sunlight is not attenuated by the Earth's atmosphere, collection is not influenced by the day-night cycle and the SPS has higher end-to-end efficiency [2-3].

Currently, different SPS concepts have been proposed by NASA, JAXA, ESA, CAST and others [4-8]. While most of the works focus on system design aspects, very few deal with technical issues, such as SPS orbit design, attitude dynamics and control, and in-orbit assembly. To achieve maximum efficiency, it is firstly paramount to ensure that the SPS is in a stabilized Sun-pointing configuration. Mankins suggests that the SPS requires a three-axis attitude stabilized approach to maintain continuous Sun tracking of the solar array [2]. Oglevie investigated a wide variety of SPS control techniques, such as space-constructed momentum wheels, gravity-gradient stabilization and various reaction control thruster typologies [9]. An integrated orbit and attitude control system of the Abacus SPS located in geostationary Earth orbit (GEO) was devised by Wie and Roithmayr [10]. In this work, perturbations were included and a PID controller plus filter was designed for continuous sun-pointing. McNally et al. proposed a new geosynchronous Laplace-plane orbit (GLP) [11], and then discussed the attitude dynamics and sun-pointing control of the SPS located in the GEO and GLO respectively [12]. In order to resolve the angular-momentum storage problem, a quasi-inertial sun-pointing control was developed by Elrod [13], and further investigated by Juang and Wang [14], and Wie and Roithmayr [10]. Zhou and Fan studied an active vibration control of a tethered SPS during attitude maneuvers [15]. Although the above works provide interesting results for SPS attitude dynamics and sun-pointing control, the two issues are still not fully addressed and resolved. On the one hand, the SPS has a very large area and mass, and is expected to be operational for more than 30 years. Hence the attitude motion could be significantly affected by perturbations, and very large control torques are required to perform sun-pointing maneuvers and then provide the necessary pointing accuracy and stability. In addition to this, the SPS sun-pointing dynamics are time-varying, and hence a time-varying controller to perform sun-pointing maneuvers would be more appropriate.

To advance the research in SPS sun-pointing control, the time-varying optimal linear quadratic regulator (LQR) technique is developed in this paper. The SPS sun-pointing dynamics are firstly proposed, and presented in state space form. To perform sun-pointing maneuvers, a periodically time-variant LQR controller is at first designed. To reduce the pointing errors in the presence of disturbances, a modified robust time-varying optimal controller combining LQR technique and active disturbance rejection is then proposed. A recursive algorithm to determine the appropriate control gain is developed. Numerical simulations are finally provided to illustrate the performance of the proposed controllers.

2. SPS Attitude Dynamics

2.1 SPS Coordinate Systems

This study focuses on the 1.2 GW geostationary Abacus satellite shown in Fig. 1, with a 3.2 × 3.2 km solar array platform, a 500-m-diam transmitting antenna and a 500 × 700 m rotating reflector. The mass of the reflector is less than 4% of the total mass, and therefore its contribution to the overall system mass and inertia can be neglected. This simplification in the analysis of sun-pointing maneuvers, leads to the following two simplifications. Firstly, the Abacus SPS can be treated as a single rigid body rather than a multi-body spacecraft. Secondly, the asymmetrical mass distribution of the reflector is not accounted for, and therefore the principal axes of inertia of the spacecraft with respect to the spacecraft's mass center are parallel to the roll, pitch and yaw axes. The moments of inertia for these axes are henceforth considered to be principal moments of inertia. To derive the sun-pointing dynamics model of the SPS, the following two coordinate systems shown in Fig. 2 are defined. The Earth Centered Inertial Coordinate System $\boldsymbol{N}$ (ECI) has a set of unit vectors $\{\boldsymbol{n}_1, \boldsymbol{n}_2, \boldsymbol{n}_3\}$ with $\boldsymbol{n}_1$ and $\boldsymbol{n}_3$ located on the Earth's equatorial plane and $\boldsymbol{n}_2$ perpendicular to them. The SPS Body-fixed Coordinate System $\boldsymbol{B}$ (SBF) with unit vector $\{\boldsymbol{b}_1, \boldsymbol{b}_2, \boldsymbol{b}_3\}$, is attached to the SPS with origin at the center of mass and the axes along the principal inertia axes. $\boldsymbol{R}$ is the position vector from the Earth center N^* to the SPS mass center B^*. The above data and description of a SPS system are from Ref. [10].

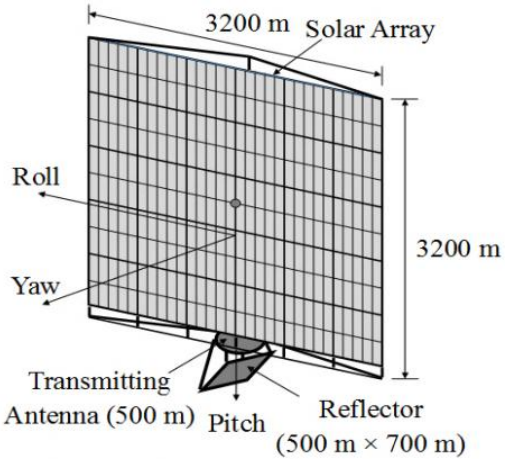

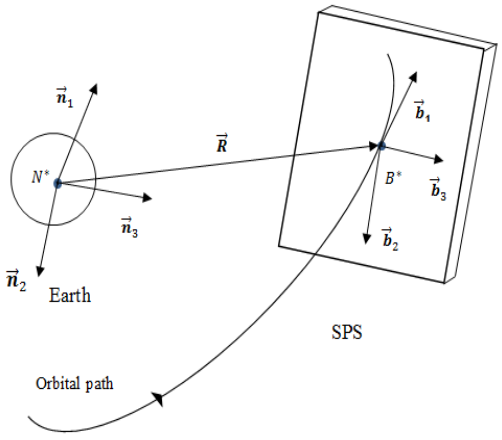

Fig. 1 Abcus SPS

Fig. 2 SPS Coordinate Systems

2.2 SPS Sun-pointing Dynamics

The SPS is considered as a huge rigid body, and the attitude dynamics is given by [10]

$$I_1\dot{\omega}_1 - (I_2 - I_3)\omega_2\omega_3 = M_1 + u_1 + d_1 \tag{1a}$$

$$I_2\dot{\omega}_2 - (I_3 - I_1)\omega_3\omega_1 = M_2 + u_2 + d_2 \tag{1b}$$

$$I_3\dot{\omega}_3 - (I_1 - I_2)\omega_1\omega_2 = M_3 + u_3 + d_3 \tag{1c}$$

where I_1, I_2 and I_3 are the principal moments of inertia, ω_1, ω_2 and ω_3 denote the angular velocity components, M_i, u_i and d_i (i=1,2,3) represent the gravity-gradient torques, control torques, and other disturbance torques respectively.

The Earth is assumed to be a sphere with uniform mass distribution, therefore the gravity-gradient torque can be expressed as follows [16]:

$$M_1 = \frac{3\mu}{R^3}(I_3 - I_2)\alpha_2\alpha_3 \tag{2a}$$

$$M_2 = \frac{3\mu}{R^3}(I_1 - I_3)\alpha_1\alpha_3 \tag{2b}$$

$$M_3 = \frac{3\mu}{R^3}(I_2 - I_1)\alpha_1\alpha_2 \tag{2c}$$

where μ is the Earth gravitational constant, R is the orbital radius of the SPS. To describe the orientation of the SPS in ECI, the Euler angles, the roll angle θ_1, the pitch angle θ_2 and the yaw angle θ_3, are defined. The rotational sequence is chosen as pitch-yaw-roll, and then the relationship between $(\boldsymbol{b}_1, \boldsymbol{b}_2, \boldsymbol{b}_3)$ and $(\boldsymbol{n}_1, \boldsymbol{n}_2, \boldsymbol{n}_3)$ is expressed as

$$\begin{bmatrix}\boldsymbol{b}_1\\ \boldsymbol{b}_2\\ \boldsymbol{b}_3\end{bmatrix} = \begin{bmatrix} C_2C_3 & S_3 & -S_2C_3 \\ -C_2S_3C_1 + S_1S_2 & C_3C_1 & S_2S_3C_1 + S_1C_2 \\ C_2S_3S_1 + C_1S_2 & -C_3S_1 & -S_2S_3S_1 + C_1C_2 \end{bmatrix}\begin{bmatrix}\boldsymbol{n}_1\\ \boldsymbol{n}_2\\ \boldsymbol{n}_3\end{bmatrix} \tag{3}$$

and α_i in Eqs.(2) are

$$\alpha_1 = -S_2C_3\cos nt - C_2C_3\sin nt \tag{4a}$$

$$\alpha_2 = (S_2S_3C_1 + S_1C_2)\cos nt - (-C_2S_3C_1 + S_1S_2)\sin nt \tag{4b}$$

$$\alpha_2 = (-S_2S_3C_1 + C_1C_2)\cos nt - (C_2S_3S_1 + C_1S_2)\sin nt \tag{4c}$$

where n is the mean motion defined as $n = \sqrt{\mu/R^3}$, $C_i = \cos\theta_i$ and $S_i = \sin\theta_i$. In stabilized mode, the Euler attitude angles and angular rates are sufficiently small, thus the attitude kinemics can be written as [10]

$$\dot{\theta}_i = \omega_i \tag{5}$$

Substituting Eqs. (2), (4) and (5) into Eq. (1) and omitting all terms of second and higher order, the linearized dynamical equations of the sun-pointing SPS are given by [10]:

$$I_1\ddot{\theta}_1 - 3n^2(I_3 - I_2)[(\cos^2 nt)\theta_1 + (\sin nt\cos nt)\theta_3] = u_1 + d_1 \tag{6a}$$

$$I_2\ddot{\theta}_2 - 3n^2(I_3 - I_1)[(\cos^2 nt - \sin^2 nt)\theta_2 + \sin nt \cos nt] = u_2 + d_2 \quad (6b)$$

$$I_3\ddot{\theta}_3 - 3n^2(I_1 - I_2)[(\sin^2 nt)\theta_3 + (\sin nt \cos nt)\theta_1] = u_3 + d_3 \quad (6c)$$

As can be seen in Eqs. (6), the pitch motion is decoupled from the roll and yaw motion, but is significantly disturbed by the time-varying gravity-gradient torque. However, the roll and yaw motions are strongly coupled due to the time-varying roll and yaw gravity-gradient torques. Other disturbances which affect SPS sun-pointing, such as the solar-radiation-pressure perturbation and the microwave-reflection perturbation, can be modeled as [10]

$$d_1 = 12000 - 11900 \cos nt \quad (7a)$$

$$d_2 = 1200 \quad (7b)$$

$$d_3 = -11900 \sin nt \quad (7c)$$

where the unit of the disturbances d_1, d_2 and d_3 is Nm.

2.3 Sun-pointing Dynamics in State Space Representation

In order to design the sun-pointing controllers, Eqs. (6) can be rewritten in the following state space representation

$$\dot{\boldsymbol{x}}_{13}(t) = \boldsymbol{A}_{13}(t)\boldsymbol{x}_{13}(t) + \boldsymbol{B}_{13}(t)\boldsymbol{f}_{13}(t) + \boldsymbol{B}_{13}(t)\boldsymbol{u}_{13} \quad (8a)$$

$$\boldsymbol{y}_{13} = \boldsymbol{C}_{13}\boldsymbol{x}_{13}(t) \quad (8b)$$

$$\dot{\boldsymbol{x}}_2(t) = \boldsymbol{A}_2(t)\boldsymbol{x}_2(t) + \boldsymbol{B}_2(t)f_2(t) + \boldsymbol{B}_2(t)u_2 \quad (8c)$$

$$\boldsymbol{y}_2 = \boldsymbol{C}_2\boldsymbol{x}_2(t) \quad (8d)$$

where $\boldsymbol{x}_{13}(t) = [\theta_1, \theta_3, \dot{\theta}_1, \dot{\theta}_3]^T$, $\boldsymbol{x}_2(t) = [\theta_2, \dot{\theta}_2]^T$, $\boldsymbol{f}_{13}(t) = [d_1, d_3]^T$, $\boldsymbol{u}_{13}(t) = [u_1, u_3]^T$, $f_2(t) = d_2 + 3n^2(I_3 - I_1)(\sin nt \cos nt)$, $\boldsymbol{B}_{13}(t) = \begin{bmatrix} 0 & 0 & {I_1}^{-1} & 0 \\ 0 & 0 & 0 & {I_3}^{-1} \end{bmatrix}$, $\boldsymbol{B}_2(t) = [0 \quad {I_2}^{-1}]^T$, $\boldsymbol{A}_2(t) = \begin{bmatrix} 0 & 1 \\ {I_2}^{-1}3n^2(I_3 - I_1)(\cos^2 nt - \sin^2 nt) & 0 \end{bmatrix}$, $\boldsymbol{C}_2(t) = [1 \quad 0]$, $\boldsymbol{C}_{13}(t) = \begin{bmatrix} 1 & 0 & 0 & 0 \\ 0 & 1 & 0 & 0 \end{bmatrix}$, $\boldsymbol{A}_{13}(t) = \begin{bmatrix} 0 & 0 & 1 & 0 \\ 0 & 0 & 0 & 1 \\ {I_1}^{-1}3n^2(I_3 - I_2)(\cos^2 nt) & {I_1}^{-1}3n^2(I_3 - I_2)(\sin nt \cos nt) & 0 & 0 \\ {I_3}^{-1}3n^2(I_1 - I_2)(\sin nt \cos nt) & {I_3}^{-1}3n^2(I_1 - I_2)(\sin^2 nt) & 0 & 0 \end{bmatrix}$. As can be seen in Eq. (8), $\boldsymbol{A}_{13}$, $\boldsymbol{A}_2$, $\boldsymbol{f}_{13}$ and $\boldsymbol{f}_2$ are actually periodically time-varying, and therefore to achieve better performance, a time-varying control technique, rather than a constant controller, would be preferable.

3. Optimal LQR Controllers Design

The LQR control technique provides a possible approach to deal with the time-varying system defined in Eq.(8). In this section, to perform sun-pointing maneuvers, the periodically time-variant LQR controllers are developed. As

the pitch motion is decoupled from the roll/yaw motion, the design of the roll/yaw controllers is performed in the following section, and the pitch controller follows the same principle and is thus omitted here.

3.1. Roll/Yaw Optimal LQR Controller

We propose the following optimal LQR controller:

$$\boldsymbol{u}_{13} = \boldsymbol{u}_0 + \boldsymbol{u}_1 \tag{9}$$

where $\boldsymbol{u}_0 = -\boldsymbol{f}_{13}$ is the feedforward controller and $\boldsymbol{u}_1 = -\boldsymbol{K}_1\boldsymbol{x}_{13}$ denotes the feedback controller. $\boldsymbol{K}_1$ can be obtained by a LQR methodology. The linear quadratic performance index is defined as

$$J_1 = \int_0^{+\infty} [\boldsymbol{x_{13}}^T \boldsymbol{Q_1} \boldsymbol{x_{13}} + \boldsymbol{u_{13}}^T \boldsymbol{R_1} \boldsymbol{u_{13}}]\, dt \tag{10}$$

where $\boldsymbol{Q_1}$ is a positive semidefinite matrix and $\boldsymbol{R_1}$ is a positive definite matrix, with both used to weigh the system state $\boldsymbol{x_{13}}$ and control input $\boldsymbol{u_{13}}$. According to optimal control theory [17], $\boldsymbol{K}_1$ is given by

$$\boldsymbol{K}_1 = \boldsymbol{R_1}^{-1} \boldsymbol{B}_{13}{}^T \boldsymbol{P}_{13}(t) \tag{11}$$

where $\boldsymbol{P}_{13}(t)$ is a positive definite symmetric matrix and is the solution of the following differential Riccati equation

$$\dot{\boldsymbol{P}}_{13}(t) = \boldsymbol{A}_{13}{}^T \boldsymbol{P}_{13}(t) + \boldsymbol{P}_{13}(t)\boldsymbol{A}_{13} - \boldsymbol{P}_{13}(t)\boldsymbol{B}_{13}\boldsymbol{R_1}^{-1}\boldsymbol{B}_{13}{}^T \boldsymbol{P}_{13}(t) + \boldsymbol{Q}_1(t) = 0 \tag{12}$$

The solution $\boldsymbol{P}_{13}(t)$ of Eq.(12) is actually periodic and can be obtained by numerical methods such as Newton-Rhapson iteration [18]. Then $\boldsymbol{K}_1$ is computed and the optimal controller (9) is defined.

3.2. Modified Optimal LQR Controller

The SPS is expected to be operational for more than 30 years, and the attitude motion could be significantly affected by the extra-large perturbations $\boldsymbol{f}_{13}(t)$ and $f_2(t)$. As can be seen in Eq.(7), these perturbations are periodic which could lead to recurring steady-state errors for the closed-loop systems Eq.(8a) and Eq.(9). To deal with this problem and improve attitude control accuracy and stability, a modified robust optimal controller combining LQR control technique and active disturbance rejection is proposed. The system block diagram is shown in Fig. 3.

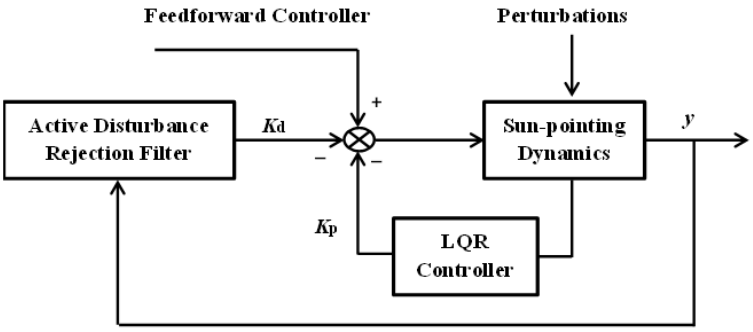

Fig. 3 System block diagram

The active disturbance rejection technique exploits the internal model principle for asymptotic disturbance rejection. Consider a periodic disturbance $d(t)$ with one or more frequency components represented as

$$d(t) = \sum A_i \sin(\omega_i t + \phi_i) \tag{13}$$

with unknown amplitudes A_i and phases ϕ_i but known frequencies ω_i. Then the disturbance rejection filter in state-space representation is described by

$$\dot{\boldsymbol{x}}_{dis} = \boldsymbol{A}_{dis}\boldsymbol{x}_{dis} + \boldsymbol{B}_{dis}\boldsymbol{y}_s \tag{14}$$

where $\boldsymbol{x}_{dis}$ is the system state introduced by the disturbance, and $\boldsymbol{y}_s$ denotes the system output. $\boldsymbol{A}_{dis}$ and $\boldsymbol{B}_{dis}$ are given by

$$\boldsymbol{A}_{dis} = \begin{bmatrix} 0 & 1 & 0 & 0 & 0 \\ -{\omega_1}^2 & 0 & 0 & 0 & 0 \\ 0 & 0 & \dots & 0 & 0 \\ 0 & 0 & 0 & 0 & 1 \\ 0 & 0 & 0 & -{\omega_i}^2 & 0 \end{bmatrix} \quad \boldsymbol{B}_{dis} = \begin{bmatrix} 0 & 1 & \dots & 0 & 0 \\ 0 & \dots & \dots & \dots & 0 \\ 0 & 0 & \dots & 0 & 1 \end{bmatrix}_{i\times 2i}^{T} \tag{15}$$

According to the standard form Eq.(13), d_1 can be rewritten as

$$d_1 = 12000 - 11900 \sin\left(nt + \frac{\pi}{2}\right) \tag{16}$$

Then the roll/yaw disturbance rejection filter is given by

$$\dot{\boldsymbol{x}}_d = \boldsymbol{A}_d\boldsymbol{x}_d + \boldsymbol{B}_d\boldsymbol{y}_{13} \tag{17}$$

where $\boldsymbol{x}_d = [x_{d1} \quad \dot{x}_{d1} \quad x_{d3} \quad \dot{x}_{d3}]^T$, $\boldsymbol{A}_d = \begin{bmatrix} 0 & 1 & 0 & 0 \\ -n^2 & 0 & 0 & 0 \\ 0 & 0 & 0 & 1 \\ 0 & 0 & -n^2 & 0 \end{bmatrix}$, $\boldsymbol{B}_d = \begin{bmatrix} 0 & 1 & 0 & 0 \\ 0 & 0 & 0 & 1 \end{bmatrix}^T$. Combining Eqs.(8a), (8b) and (17) yields:

$$\dot{\boldsymbol{x}} = \boldsymbol{A}\boldsymbol{x}(t) + \boldsymbol{B}\boldsymbol{f}(t) + \boldsymbol{B}\boldsymbol{u}(t) \tag{18}$$

where $\boldsymbol{A} = \begin{bmatrix} \boldsymbol{A}_{13} & \boldsymbol{0} \\ \boldsymbol{B}_d C_{13} & \boldsymbol{A}_d \end{bmatrix}$, $\boldsymbol{B} = [\boldsymbol{B}_{13}{}^T \quad \boldsymbol{0}]^T$, $\boldsymbol{B} = [\boldsymbol{x}_{13}{}^T \quad \boldsymbol{x}_d{}^T]^T$, $\boldsymbol{f}(t) = \boldsymbol{f}_{\boldsymbol{13}}(t)$. Then the modified optimal controller is given by:

$$\boldsymbol{u} = \boldsymbol{u}_0 + \boldsymbol{u}_2 \tag{19}$$

where $\boldsymbol{u}_2 = -\boldsymbol{K}_2\boldsymbol{x} = -[\boldsymbol{K}_p \quad \boldsymbol{K}_d]\begin{bmatrix} \boldsymbol{x}_{13} \\ \boldsymbol{x}_d \end{bmatrix}$, $\boldsymbol{K}_p$ is the gain matrix of system state $\boldsymbol{x}_{13}$ and $\boldsymbol{K}_d$ denotes the gain matrix of $\boldsymbol{x}_d$. Therefore, we redefine the linear quadratic performance index as

$$J_2 = \int_0^{+\infty} [\boldsymbol{x}^T \boldsymbol{Q}_2 \boldsymbol{x} + \boldsymbol{u}^T \boldsymbol{R}_2 \boldsymbol{u}]\, dt \tag{20}$$

where $\boldsymbol{Q}_2$ and $\boldsymbol{R}_2$ are positive definite weight matrices. $\boldsymbol{K}_2$ can be calculated by:

$$\boldsymbol{K}_2 = \boldsymbol{R}_2{}^{-1} \boldsymbol{B}^T \boldsymbol{P}_2(t) \tag{21}$$

where $\boldsymbol{P}_2(t)$ is a positive definite symmetric matrix and is the solution to the following differential Riccati equation

$$\dot{\boldsymbol{P}}_2(t) = \boldsymbol{A}^T \boldsymbol{P}_2(t) + \boldsymbol{P}_2(t)\boldsymbol{A} - \boldsymbol{P}_2(t)\boldsymbol{B}\boldsymbol{R}_2{}^{-1}\boldsymbol{B}^T \boldsymbol{P}_2(t) + \boldsymbol{Q}_2(t) = 0 \tag{22}$$

As can be seen, the solution $\boldsymbol{P}_2$ of the periodic Riccati equation Eq.(22) is the key to achieving the proposed optimal controller Eq.(19). An analytical solution of Eq.(22) cannot be obtained hence a recursive algorithm to solve the periodic Riccati differential equation and obtain optimal controller has been developed. The proposed recursive algorithm includes two steps: the structure-preserving computation of state transition matrix and the periodic condition, and is presented in the following section.

3.3. Solution of Periodic Riccati Differential Equation

Let $\boldsymbol{H}(t)$ represent the periodic time-varying Hamiltonian matrix corresponding to the coefficient matrices of the periodic Riccati equation (22), and given by:

$$\boldsymbol{H}(t) = \begin{bmatrix} \boldsymbol{A}(t) & \boldsymbol{R}(t) \\ \boldsymbol{Q}_2(t) & -\boldsymbol{A}^T(t) \end{bmatrix} \tag{23}$$

where $\boldsymbol{R} = \boldsymbol{B}\boldsymbol{R}_2{}^{-1}\boldsymbol{B}^T$. The Hamiltonian matrix $\boldsymbol{H}(t)$ satisfies the following initial value problem of the linear ordinary differential equation:

$$\dot{\boldsymbol{U}}(t,0) = \boldsymbol{H}(t)\boldsymbol{U}(t,0), \boldsymbol{U}(0,0) = \boldsymbol{E} \tag{24}$$

where $\boldsymbol{E}$ is an identity matrix. Eq.(24) can be integrated from $t = 0$ to $t = T$ using any standard numerical integration method for ordinary differential equation. However, this direct integration method for the transition matrix $\boldsymbol{U}(T,0)$ has several potential numerical difficulties for long periods and/or unstable dynamics system associated with the

Hamiltonian matrix $\boldsymbol{H}(t)$ as mentioned in Ref.[19]. Therefore, to deal with this problem, the transition matrix $\boldsymbol{U}(T,0)$ will be computed by the following product form

$$\boldsymbol{U}(T,0)=\boldsymbol{U}(T,T-\eta)*\ldots*\boldsymbol{U}(2\eta,\eta)\boldsymbol{U}(\eta,0) \tag{25}$$

where $\eta=T/N$ denotes the integration step-length and N is the sub-intervals number. Besides, each interval transition matrix is a symplectic one, such that

$$\boldsymbol{U}^{T}(k\eta,(k-1)\eta)\boldsymbol{V}\boldsymbol{U}(k\eta,(k-1)\eta)=\boldsymbol{V} \tag{26}$$

where $\boldsymbol{V}=\begin{bmatrix}\boldsymbol{0} & \boldsymbol{E}\\ -\boldsymbol{E} & \boldsymbol{0}\end{bmatrix}$. Therefore, in order to preserve the symplectic character of the interval transition matrices $\boldsymbol{U}(k\eta,(k-1)\eta)$, $k=1,2\ldots N$, the structure-preserving methods, such as Magnus series method [19], can be employed for the computation of the above interval transition matrices.

Actually, $\boldsymbol{U}(k\eta,(k-1)\eta)$ describes the following relationship between two adjacent time points $k\eta$ and $(k-1)\eta$

$$\begin{cases}\boldsymbol{z}_{k+1}=\boldsymbol{U}^{11}(k\eta,(k-1)\eta)\boldsymbol{z}_{k}+\boldsymbol{U}^{12}(k\eta,(k-1)\eta)\boldsymbol{v}_{k}\\ \boldsymbol{v}_{k+1}=\boldsymbol{U}^{21}(k\eta,(k-1)\eta)\boldsymbol{z}_{k}+\boldsymbol{U}^{22}(k\eta,(k-1)\eta)\boldsymbol{v}_{k}\end{cases} \tag{27}$$

where $\boldsymbol{z}_k$ and $\boldsymbol{v}_k$ are the state matrices, and $\boldsymbol{U}$ is given by

$$\boldsymbol{U}(k\eta,(k-1)\eta)=\begin{bmatrix}\boldsymbol{U}^{11}(k\eta,(k-1)\eta) & \boldsymbol{U}^{12}(k\eta,(k-1)\eta)\\ \boldsymbol{U}^{21}(k\eta,(k-1)\eta) & \boldsymbol{U}^{22}(k\eta,(k-1)\eta)\end{bmatrix} \tag{28}$$

In optimal control theory, $\boldsymbol{z}_k$ denotes the original state variable and $\boldsymbol{v}_k$ is the dual state variable. Furthermore, Eq.(27) can also be rewritten as [19, 20]

$$\begin{cases}\boldsymbol{z}_{k}=\boldsymbol{F}(k\eta,(k-1)\eta)\boldsymbol{z}_{k-1}+\boldsymbol{G}(k\eta,(k-1)\eta)\boldsymbol{v}_{k}\\ \boldsymbol{v}_{k+1}=-\boldsymbol{S}(k\eta,(k-1)\eta)\boldsymbol{z}_{k-1}+\boldsymbol{F}^{T}(k\eta,(k-1)\eta)\boldsymbol{v}_{k}\end{cases} \tag{29}$$

where $\boldsymbol{F}$, $\boldsymbol{G}$ and $\boldsymbol{S}$ are sub-interval mixed energy matrices, and

$\boldsymbol{G}(k\eta,(k-1)\eta)=\boldsymbol{U}^{12}(k\eta,(k-1)\eta)\{\boldsymbol{U}^{22}(k\eta,(k-1)\eta)\}^{-1}$, $\boldsymbol{F}(k\eta,(k-1)\eta)=\{\boldsymbol{U}^{22}(k\eta,(k-1)\eta)\}^{-T}$, $\boldsymbol{S}(k\eta,(k-1)\eta)=\{\boldsymbol{U}^{22}(k\eta,(k-1)\eta)\}^{-1}\boldsymbol{U}^{21}(k\eta,(k-1)\eta)$. According to Ref.(18), we can obtain the recurrence formula

$$\boldsymbol{P}_{k-1}=\boldsymbol{S}(k\eta,(k-1)\eta)+\boldsymbol{F}^{T}(k\eta,(k-1)\eta)\boldsymbol{P}_{k}(\boldsymbol{I}+\boldsymbol{G}(k\eta,(k-1)\eta)\boldsymbol{P}_{k})^{-1}\boldsymbol{F}(k\eta,(k-1)\eta) \tag{30}$$

Let $\boldsymbol{P}_{k-1}=\boldsymbol{P}_0$ and $\boldsymbol{P}_k=\boldsymbol{P}_T$, and the periodic condition is given by

$$\boldsymbol{P}_0=\boldsymbol{P}_T \tag{31}$$

Then Eq.(30) can be rewritten as following algebra Riccati equation

$$\boldsymbol{P}_0=\boldsymbol{S}(T,0)+\boldsymbol{F}^{T}(T,0)\boldsymbol{P}_0(\boldsymbol{I}+\boldsymbol{G}(T,0)\boldsymbol{P}_0)^{-1}\boldsymbol{F}(T,0) \tag{32}$$

The initial solution $\boldsymbol{P}_0$ of the periodic Riccati differential equation (24) can be computed by solving the algebra Riccati equation (32). Then, every solution $\boldsymbol{P}_k$ at time point t_k can be obtained based on the recurrence formula Eq.(30). Hence, the controller $\boldsymbol{K}_2$ is finally defined.

4. Numerical Results

In this section, numerical results are presented to illustrate and evaluate the theoretical concepts introduced above. The principal moments of inertia are $I_1 = 2.8 \times 10^{13}$ kg·m^2, $I_2 = 1.8 \times 10^{13}$kg·m^2 and $I_3 = 4.6 \times 10^{13}$kg·m^2 [10]. For the roll/yaw axis, the initial state is $\boldsymbol{x}_{13}(0) = [10^\circ, -10^\circ, -0.0011^\circ/\mathrm{s}, 0.0023^\circ/\mathrm{s}]^T$, and the weight matrices by trial and error are chosen as $\boldsymbol{Q}_2 = diag(0.004,0.004,42,40,0.004,40,0.004,41)$, $\boldsymbol{R}_2 = diag(17.51,70.62)$. For the pitch axis, the initial state is $\boldsymbol{x}_2(0) = [10^\circ, -0.0029^\circ/\mathrm{s}]^T$, and the weight matrices are then given by $\boldsymbol{Q}_2{}' = diag(0.004,400,0.004,400)$, $\boldsymbol{R}_2{}' = 0.2405$. The following constant controllers including PID feedback plus disturbance rejection filter are also provided to compare the performance with proposed time-varying LQR controller Eq.(19).

$$u_{\mathrm{roll}} = -\left(9 \times 10^9 s + 8 \times 10^5 + \frac{7}{s}\right)\frac{2.04\times10^8 s^2+8.57\times10^3 s+1}{1.88\times10^8 s^2+1}\theta_1(s) \tag{33a}$$

$$u_{\mathrm{pitch}} = -\left(8 \times 10^9 s + 6 \times 10^5 + \frac{1}{s}\right)\frac{4.82\times10^7 s^2+4.17\times10^3 s+1}{4.17\times10^7 s^2+1}\theta_2(s) \tag{33b}$$

$$u_{\mathrm{yaw}} = -\left(7 \times 10^9 s + 3 \times 10^5 + \frac{1}{200s}\right)\frac{2.04\times10^8 s^2+8.57\times10^3 s+1}{1.88\times10^8 s^2+1}\theta_3(s) \tag{33c}$$

In the following simulation cases, $\pm 10\%$ uncertainties of moments of inertia and disturbances are taken into account, and the results are given below.

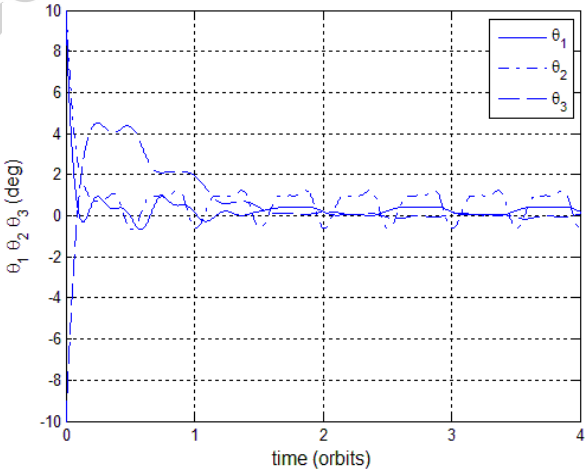

Fig. 4 The Euler angles θ_1, θ_2 and θ_3 — controller (9)

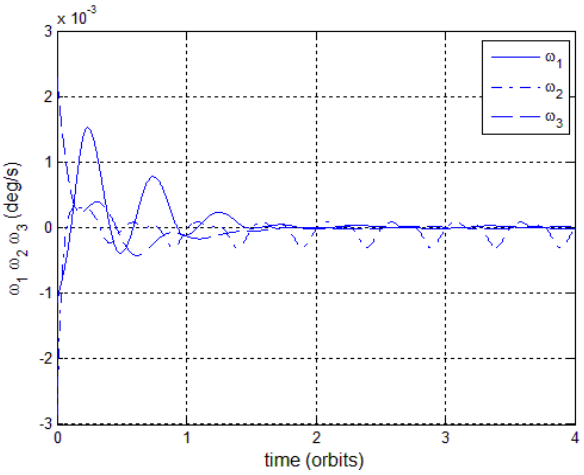

Fig. 5 The angular velocities ω_1, ω_2 and ω_3 — controller (9)

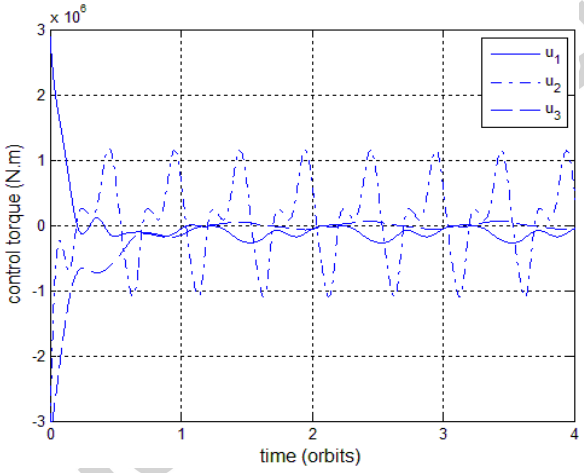

Fig.6 Control torques u_1, u_2 and u_3 — controller (9)

The results by employing the time-varying optimal LQR controller (9) are firstly presented in Figs. 4-6. As can be seen, the Euler angles θ_1 and θ_3 converge to $\pm 0.5^{\circ}$, while θ_2 can only converge to $\pm 1^{\circ}$ in the presence of large disturbances and uncertainties. The steady-state error of θ_2 and ω_2 can be observed in its periodic oscillation. This is due to the periodic gravity-gradient torque in pitch axis mentioned above. The control torques are presented in Fig.6, with maximum magnitude at $\pm 3 \times 10^6$ Nm at the start of the maneuver.

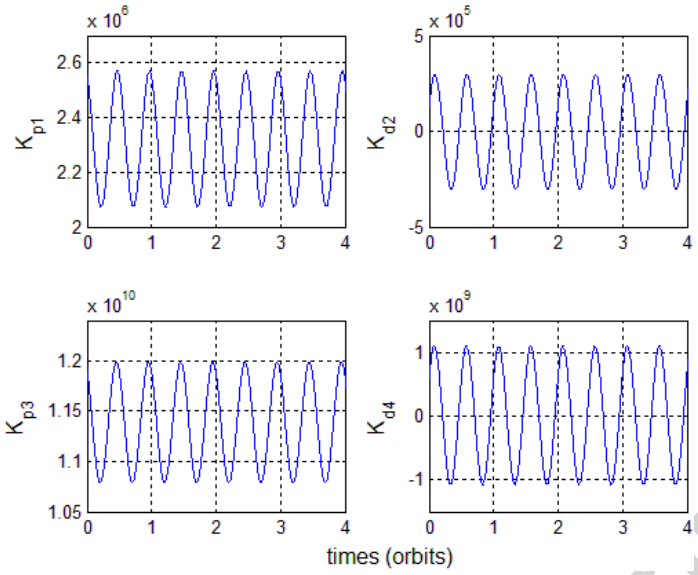

Fig.7 The components of time-varying controller gain $\boldsymbol{K}_2$

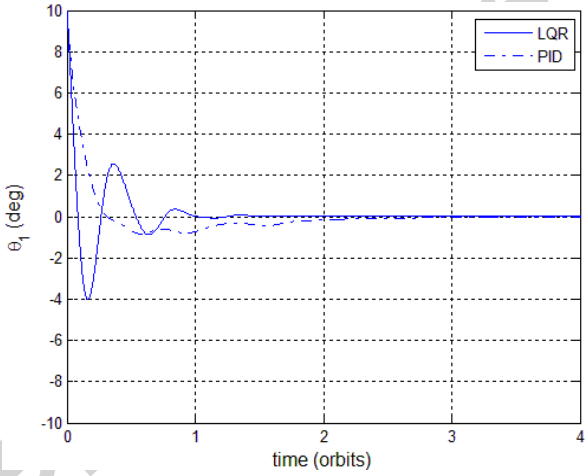

Fig.8 The roll angle θ_1

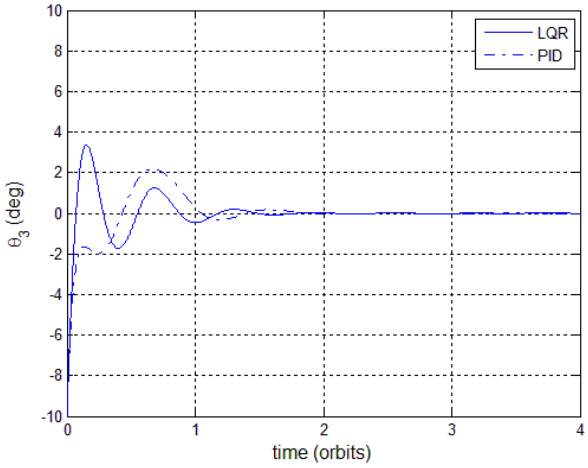

Fig.9 The yaw angle θ_3

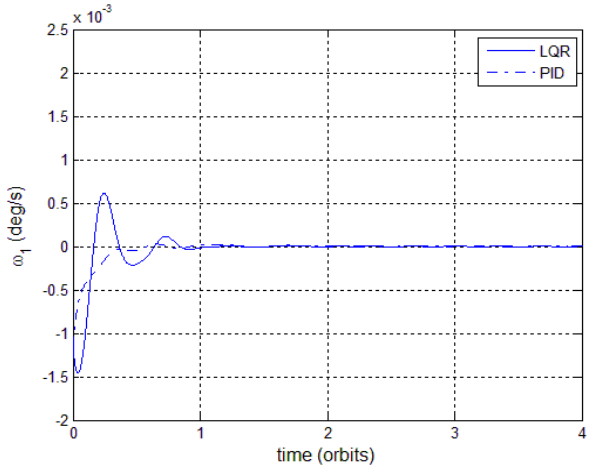

Fig.10 The roll angular velocity ω_1

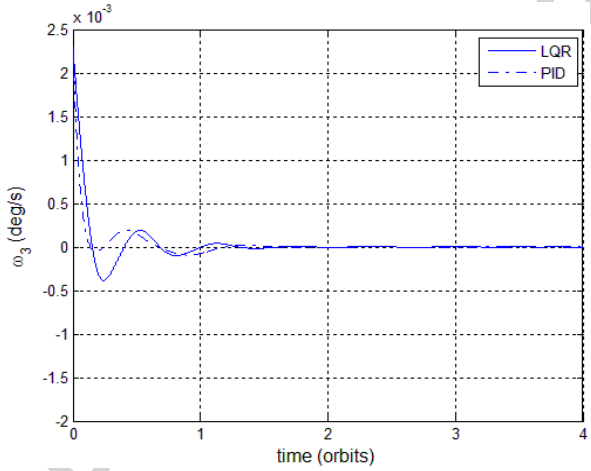

Fig.11 The yaw angular velocity ω_3

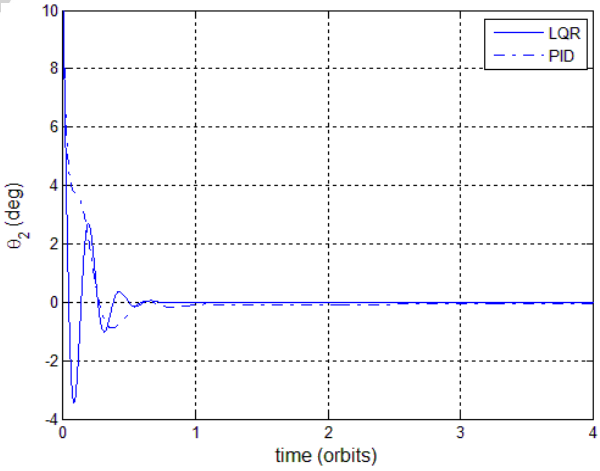

Fig.12 The pitch angle θ_2

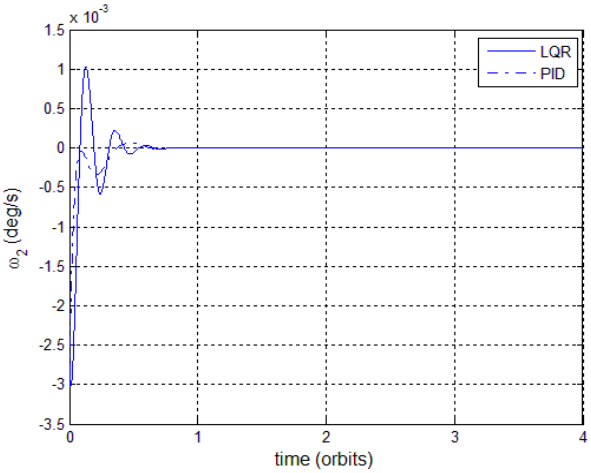

Fig.13 The pitch angular velocity ω_2

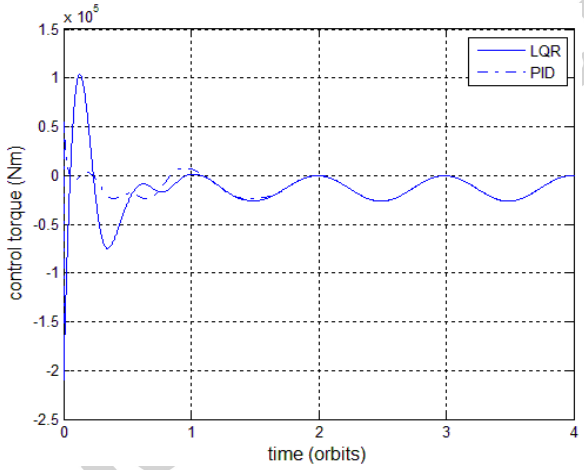

Fig.14 Roll control torques

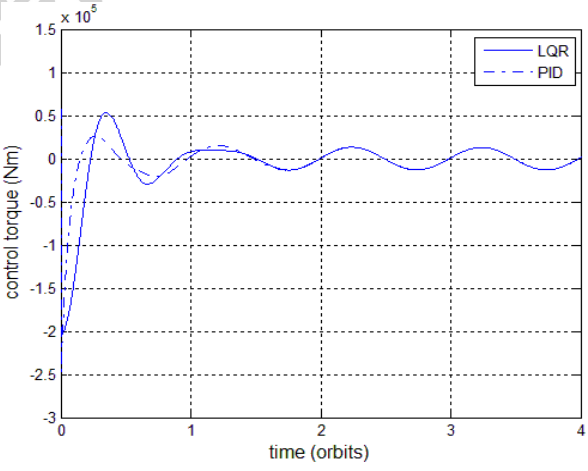

Fig.15 Yaw control torques

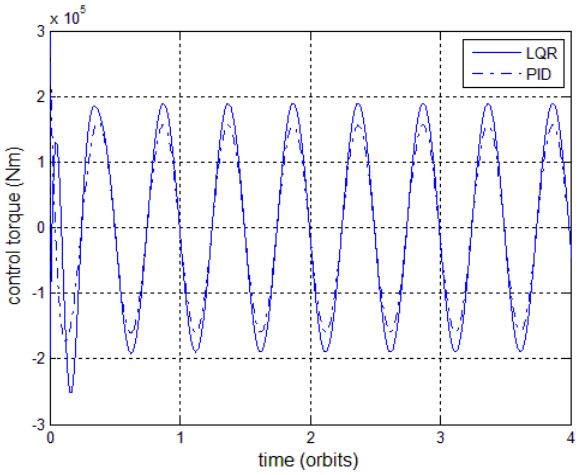

Fig.16 Pitch control torques

Comparison of the results of the time-varying robust optimal LQR controller (19) and the constant controllers Eqs.(33) are shown in Figs. 7-16, where the solid lines represent the results under the time-varying LQR controllers (19) and the dash-dot lines denote the results under a constant PID controller (33). Fig. 7 presents the components of time-varying controller gain $\boldsymbol{K}_2$. Actually, K_{p1} and K_{p3} are the controller gains of system states θ_1 and $\dot{\theta}_1$, and K_{d2} and K_{d4} denote the gains of $\dot{x}_{\mathrm{d1}}$ and $\dot{x}_{\mathrm{d3}}$. As shown, $\boldsymbol{K}_2$ is periodic time-varying, such that the proposed controller (19) provides more appropriate torques to perform sun-pointing maneuvers. The angles and angular velocities of sun-pointing maneuvers are given in Figs. 8-13. As can be clearly seen, θ_1, θ_2 and θ_3 have a faster convergence rate under a time-varying LQR controller (19). From Figs. 8&10, we can see that the steady-state errors of θ_1 and ω_1 converge to $\pm 0.05^{\circ}$ and $\pm 2 \times 10^{-5\,\circ}/\mathrm{s}$ in 1 days (orbit periods) for controller (19), while it takes 2.5 days for controller (33). Convergence is even faster for the pitch angle θ_2 which converges to $\pm 0.05^{\circ}$ in 0.7 days with the optimal LQR controller (19), while it takes 4 days to converge to $\pm 0.055^{\circ}$ with the constant controller (33), as shown in Fig. 12. Thus, it can be seen that the optimal LQR controller (19) provides a better convergence performance in the presence of large disturbances and uncertainties. Figs. 14-16 compare the torques of two controllers (19) and (33) which have similar amplitudes. It can be seen that the control torque of pitch axis is much larger than other two axes since the pitching motion is significantly disturbed by the time-varying gravity-gradient torque. Comparing Figs.8-16 with Figs.4-6, it can be concluded that the modified optimal LQR controller (19) can effectively reduce the steady-state errors and then improve sun-pointing accuracy and stability in the presence of large disturbances and uncertainties, since the proposed controller (19) has combined time-varying LQR and active disturbance rejection techniques to deal with periodic disturbances.

It should be noted that the optimal control performance depends on the weight matrices $\boldsymbol{Q}_2$ and $\boldsymbol{R}_2$. It is still a challenging problem to reasonably and analytically choose weight matrices. Generally, we can choose larger values of $\boldsymbol{R}_2$ in order to decrease control torques. Meanwhile, larger values of $\boldsymbol{Q}_2$ leads to a smaller steady-state errors. For instance, if the weight matrices are chosen as $\boldsymbol{Q}_2 = diag(0.004, 0.004, 42, 40, 0.004, 40, 0.004, 41)$ and $\boldsymbol{R}_2 = diag(140.05,564.93)$, then the roll angle and control torque are presented in Figs 17-18. Comparing with Figs. 8&14 (solid lines), the magnitude of roll axis torque is obviously reduced by increasing $\boldsymbol{R}_2$, which is highly

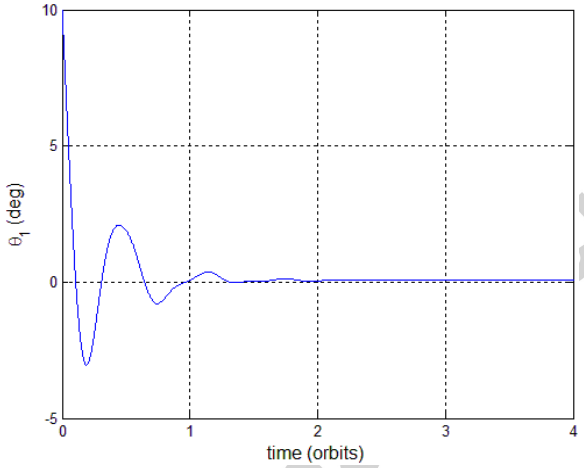

Fig.17 The roll angle θ_1

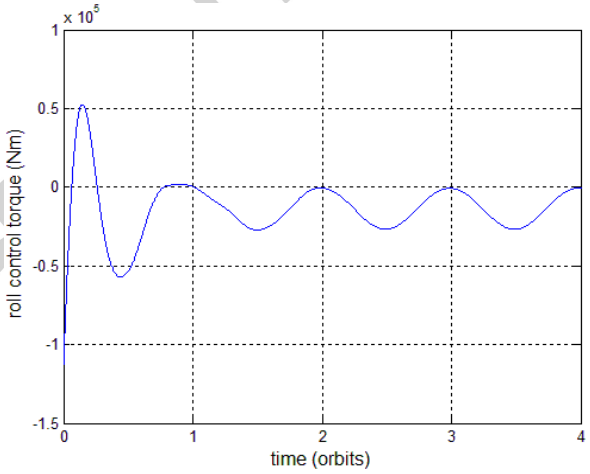

Fig.18 Roll control torques

desirable. While the roll angle θ_1 converges to $\pm 0.1^{\circ}$ in 2 days. Meanwhile, the higher control accuracy of θ_1 can be achieved if a larger value of $\boldsymbol{Q}_2$ is chosen, but the control torques will greatly increase.

5. Future Work

In Ref.(9) and this paper, the SPS is considered as a huge rigid body. The SPS has however a significantly high area-to-mass ratio (HAMR) compared with conventional spacecraft, which could bring about the flexible characteristics for such a SPS. These are large-scale, massive, but thin structures, so structural bending and flexing may occur during on-orbit operations and attitude maneuvers. Besides, this could lead to changes in the effects of orbital perturbations and hence attitude control. Future studies can also be performed to address the attitude dynamics and sun-pointing/microwave-beam control for such a HAMR flexible SPS.

Due to their mass, SPS require large control torques to minimise various disturbances when performing attitude maneuvers. Employing one or several actuators, such as flywheels or CMGs, is obviously not a viable option for controlling such a large space structure. The current approach is to use a large number of ion thrusters as the main actuators for SPS control. Hence the distributed control approach of such thrusters, to achieve integrated orbit and attitude maneuvers, appears to be another interesting avenue for future work.

6. Conclusion

The robust optimal sun-pointing control of a geostationary solar power satellite has been investigated in this paper. The sun-pointing dynamics are firstly presented in the state space representation. Due to the time-varying characteristics of the dynamic model, a periodically time-varying LQR controller, to determine the pointing accuracy and the control inputs, is designed to perform the sun-pointing maneuver. A modified optimal time-varying controller, combining LQR technique and disturbance rejection filter, is then developed to reduce the periodic steady-state errors caused by disturbances, and therefore improve pointing accuracy and stability. To solve the time-varying control gain, a recursive algorithm is proposed. The numerical results demonstrate that the optimal time-varying controller has a faster convergence rate than a constant controller, and achieves higher control accuracy.

Acknowledgments

This work is supported by the National Natural Science Foundation of China under Grant nos. 11502040 & 11432010, and the Fundamental Research Funds for the Central Universities (DUT15LK31).

References

[1] P. E. Glaser, Power from the Sun: its future, Science. 162(3856) (1968) 857-861.

[2] J. C. Mankins, K. Nobuyuki, Space Solar Power: The first international assessment of space solar power: Opportunities, issues and potential pathways forward, International Academy of Astronautics, Paris,2011.

[3] D. V. Smitherman, A comparison of a solar power satellite concept to a concentrating solar power system, in: AIAA SPACE 2013 Conference and Exposition, San Diego, CA, 2013.

[4] C. Carrington, J. Fikes, M. Gerry, D. Perkinson, H. Feingold, J. Olds, The Abacus/Reflector and integrated symmetrical concentrator: concepts for space solar power collection and transmission, in: 35th AIAA, ASME, IEEE, et al, Intersociety Energy Conversion Engineering Conference and Exhibit, Las Vegas, NV, 2000.

[5] M. Nagamoto, S. Sasaki, Y. Naruo, Conceptual study of a solar power satellite, SPS 2000, in: 19th International Symposium on Space Technology and Science, Yokohama, Japan, 1994.

[6] H. Matsumoto, K. Hashimoto, Report of the URSI inter-commission working group on SPS, URSI, 2007.

[7] X. B. Hou, L. Wang, X. H. Zhang, L. Zhou. Concept design on multi-rotary joints SPS, Journal of Astronautics, 36(11) (2015) 1332-1338.

[8] Q. B. Jin, J. Huang, J. Y. Fan, Motion analysis and trajectory planning of solar tracking of a class of Space Solar Power Station, Sol. Energy. 122 (2015) 239-248.

[9] R. E. Oglevie, Attitude control of large solar power satellites, in: AIAA Guidance and Control Conference, Palo Alto, CA, 1978.

[10] B. Wie, C. M. Roithmayr, Attitude and orbit control of a very large geostationary solar power satellite, J. Guid. Control. Dynam. 28(3) (2005) 439-451.

[11] I. McNally, D. Scheeres, G. Radice, Locating large solar power satellites in the Geosynchronous laplace plane, J. Guid. Control. Dynam. 38(3) (2015) 489-505.

[12] I. McNally, D. Scheeres, G. Radice, Attitude dynamics of large geosynchronous solar power satellites, in: AIAA/AAS Astrodynamics Specialist Conference, San Diego, CA, 2014.

[13] B. D. Elrod, A quasi-inertial attitude mode for orbit spacecraft, J. Spacecraft. Rockets. 9(12) (1972) 889-895.

[14] J. N. Juang, S. J. Wang, An investigation of quasi-inertial attitude control for a solar power satellite, Space Solar Power Review, 3(4) (1982) 337-352.

[15] D. Zhou, J. Fan, Active vibration control of tethered solar power satellite during attitude maneuvering, Journal of Astronautics, 33 (2012) 605-611.

[16] D. Liu, J. Zhao, Space vehicle dynamics, Harbin Institute of Technology Press, Harbin, 2003.

[17] D Xue, Computer Aided control system design using Matlab language, TsingHua University Inc. Beijing, 2012.

[18] H. J. Peng, G. Z. Wu, W. X. Zhong, Fourier expansion based recursive algorithms for periodic Riccati and Lyapunov matrix differential equations, J. Comput. Appl. Math. 235(12) (2011) 3571-3588.

[19] H. J. Peng, G. Z. Wu, W. X. Zhong, H∞ Norm computation of linear continuous-time periodic systems by a structure-preserving algorithm, Int. J. Control. 87(1) (2014) 131-142.

[20] Z. Cai, J. Zhao, H. Peng, et al, Nonlinear control of rotating multi-tethered formations in halo orbits, Int. J. Comp. Meths. 11(supp01) (2014) 1344008.

Highlights

- A robust optimal time-varying controller is designed to improve pointing accuracy.
- The sun-pointing dynamics and the filter are proposed in state space representation.
- A recursive algorithm to solve controller gain matrix is developed.